

Mapping H₂ Excitation and Mass across NGC 5194 with the Spitzer IRS

Gregory Brunner^{1,2}

Department of Physics and Astronomy, Rice University,
Houston, TX 77005

gbrunner@ipac.caltech.edu, gbrunner@rice.edu

Kartik Sheth³, Lee Armus³, and George Helou³

Spitzer Science Center, Pasadena, CA 91125

Eva Schinnerer⁴

Max-Planck-Institüt für Astronomie, Heidelberg, Germany

and

Stuart Vogel⁵ and Mark Wolfire⁵

Department of Astronomy, University of Maryland, College Park, MD 20741

Received _____; accepted _____

¹Department of Physics and Astronomy, Rice University, Houston, TX 77005

²Visiting Graduate Student Fellow, Spitzer Science Center, Caltech, Pasadena, CA

³Spitzer Science Center, Caltech, Pasadena, CA

⁴Max-Planck-Institüt für Astronomie, Heidelberg, Germany

⁵Department of Astronomy, University of Maryland, College Park, MD

ABSTRACT

Subject headings: galaxies: ISM — galaxies: H₂ — galaxies: individual(NGC 5194)

1. Introduction

Galactic evolution is inherently correlated with molecular hydrogen (H_2) within a galaxy. In the Milky Way Galaxy, we observe H_2 in dense molecular clouds. The collapse of these molecular clouds triggers bursts of star formation. In other galaxies, we observe molecular gas trigger star formation in spiral arms via the passage of a spiral density wave (Vogel et al. 1983), within nuclear regions of galaxies (Young and Deveraux 1991), and at the ends of bars in barred spiral galaxies (Sheth et al. 2000). Thus, H_2 serves as the fuel for star formation and is fundamentally connected with galaxy evolution.

The Whirlpool Galaxy (M51a, NGC 5194) is a nearby, face-on galaxy that has been extensively studied in X-rays (Palumbo et al. 1985, Terashima et al. 2001); UV, optical (Scoville et al. 2001), and IR (Calzetti et al. 2005); submillimeter (Matsushita et al. 2004); millimeter (Helfer and Blitz 1997); and radio wavelengths (Murphy et al. 2005). At a distance of 9.6 Mpc (Sandage and Tamman, 1975), its proximity, orientation, and morphology make it an ideal target to study the interstellar medium (ISM) across distinct dynamical, chemical, and physical environments in a galaxy. Studies have revealed variations in CO emission and UV radiation field, metallicity gradients, and temperature across the galaxy. Thus, it has been called a *Rosetta Stone* for galaxy evolution (Scoville and Young, 1983).

The Spitzer Space Telescope Infrared Spectrograph (IRS) (Houck et al. 2004) is a powerful tool for observing the H_2 within galaxies and thus deciphering the evolution of M51a. The Spitzer IRS low resolution modules cover 5 - 38 μm (SL, 5 - 14 μm ; LL, 14 - 38 μm) giving observers access to the lowest pure rotational lines of H_2 . These lines trace the warm ($T = 100 - 1000 K$) molecular gas and are important diagnostics of the ISM allowing for the determination of the H_2 excitation-temperature, mass, and ortho-to-para ratio of H_2 . Thus, by understanding the pure rotational H_2 line emission from a galaxy, constraints can

be placed on the energy injection mechanisms (i.e. radiative heating, shocks, turbulence) that heat the molecular gas phases in the ISM.

In this paper, we present spatially resolved observations of the H₂ rotational lines across a radial strip of NGC 5194. Using the Spitzer IRS, we have spectrally mapped a radial strip (295" x 51" in the long low module and 324" x 57" in the short low module) across NGC 5194 in order to understand the conditions of the warm (T = 100 -1000 K) molecular ISM across dynamically distinct environments. From the spatially resolved IRS low resolution spectra, maps of emission from the six lowest pure rotational transitions of H₂, the H₂(0-0)S(0) (28.22 μ m), H₂(0-0)S(1) (17.04 μ m), H₂(0-0)S(2) (12.28 μ m), H₂(0-0)S(3) (9.66 μ m), H₂(0-0)S(4) (8.02 μ m), and H₂(0-0)S(5) (6.91 μ m) lines were created. These maps represent measurements of extinction corrected line flux across NGC 5194 (presented in §3.1). Maps are used to determine the spatial distribution of the H₂ excitation-temperature and mass across the galaxy(§3.2). The dominant excitation mechanism of H₂ (photodissociation by UV photons, shocks, and/or x-ray dissociation) is determined in various regions across the galaxy by comparing the H₂ distribution to CO (J = 1 - 0) emission (§4.2), [OIV](25.89 μ m) emission (§4.3), and x-ray emission (§4.4).

2. Observations, Data Reduction, and Analysis

2.1. Spectral Data

Spectra were obtained for NGC 5194 using the two low-resolution modules of the Infrared Spectrograph in spectral mapping mode. In spectral mapping mode, we moved the IRS in a series of discrete steps settling at each position before beginning integration. Half slit spacing were used for all integrations. Integration times in the SL and LL were 14.6 s. Each slit position was covered twice. In total, 1,412 spectra were taken in the

SL while 100 were taken in the LL (including background observations). SL integrations were taken perpendicular to the LL integrations in accordance with the SINGS radial strip mapping strategy specified in by Kennicutt et al (2003). Further details on the observation strategy are available on SST’s Leopard for project ID 200138 (PI: K. Sheth). Dedicated off source background observations were taken for the SL observations. Backgrounds for the LL observations were taken from outrigger data collected while the spacecraft was mapping in the adjacent module.

The spectra were assembled from the basic calibration data into spectral cubes for each module using CUBISM (Smith et al. 2007, in preparation). CUBISM allows for the assembly of cubes, extraction of spectra, and creation of spectral maps. Background subtraction and bad pixel removal was done within CUBISM. The individual IRS spectra were processed using version S14.0 of the Spitzer Science Center pipeline.

Spectral maps of the H₂S(0) - H₂S(5) lines were created with PAHFIT (Smith et al. 2007), a robust mid-infrared spectral fitting routine. PAHFIT decomposes an IRS low resolution spectrum allowing the recovery of the full flux of blended features. This allows the recovery of the full line flux of the H₂ features, including severely blended lines such as H₂S(1), blended with the 17 μm PAH complex (Smith et al. 2004); H₂S(2), blended with [NeII](12.8 μm); and H₂S(5), blended into [ArII](6.9 μm).

In order to run PAHFIT though the SL and LL data cubes, the grid of the SL1 data cube was interpolated to the grid of the SL2 data cube. The data cubes were then concatenated into one SL cube. The same procedure was used to concatenate the LL1 and LL2 data cubes into one LL data cube. In regions where the first order (SL1, LL1) spectra overlapped with the second order (SL2, LL2) spectra, the first order spectra were scaled up to the second order spectra. The concatenated data cubes were then smoothed spatially by a 3x3 box to increase the signal to noise ratio of spectra. Grouping spectra was also done to

avoid pixel aliasing, which has the affect of creating a saw-tooth pattern in the continuum (CUBISM User Manual). PAHFIT was then run through both the SL and LL data cubes. The SL data cube was fit separately from the LL data cube.

PAHFIT decomposes every spectrum in both the SL and LL data cubes. In doing so, PAHFIT returns fit parameters to the specified features in the spectrum. These parameters include extinction corrected integrated line flux, line FWHM, line equivalent width, and uncertainty. The integrated flux measurements are extinction corrected within PAHFIT (see Smith et al. 2007 for the extinction curve). While running PAHFIT through the data cubes, information concerning the position of each spectrum was retained. This allows for the reconstruction of spectral feature (PAH, H₂, ionization line) maps from the results of PAHFIT. When using PAHFIT on an entire data cube, maps of every feature specified by PAHFIT were returned. Additionally, the fit to each spectrum was retained and the fit to the continuum was reconstructed from internal PAHFIT functions. From these two data cubes, a residual data cube and a continuum subtracted data cube were created for both the SL and LL data cubes. These data cubes are crucial in determining the consistency of the fitted spectra. In order to check the accuracy of the map of H₂S(3) integrated flux, it was compared it to the image created from the continuum subtraction to the SL data cube.

In using PAHFIT, the default values for the temperatures of the starlight and eight thermal dust continuum components were used to fit the continuum. Additionally, the optical depth of the dust extinction at 9.7 μm and 18 μm were also fit. This was especially important in recovering an accurate measurement of the H₂S(3) 9.6 μm line in the 9.7 μm silicate absorption trough.

2.2. CO Map

The BIMA (Berkely Illinois Maryland Array) CO (J=1-0) map was acquired as a part of the BIMA Survey of Nearby Galaxies (SONG) (Regan et al. 2001; Helfer et al. 2003). The CO map was mosaicked from 26 fields. The beam size is 5.8 x 5.1 arcsec (220 x 190 pc), the velocity channel width is 10 km s⁻¹, and the root-mean-square (rms) noise level is 61 mJy beam⁻¹.

2.3. X-ray Emission

The map of x-ray emission from M51 was observed by the Advanced CCD Imaging Spectrometer (ACIS) on the *Chandra X – Ray Observatory* on 20 June 2000. The total integration time was 14,865 seconds. Further details of the observations are presented in Terashima and Wilson (2001).

3. Results and Analysis

3.1. H₂ Emission Maps

Molecular Hydrogen emission has been detected across NGC 5194. The H₂S(0), H₂S(1), H₂S(2), H₂S(3), H₂S(4), and H₂S(5) lines have been mapped across the radial strip. In figures 1 and 2, maps of the extinction corrected flux of the H₂S(0) - H₂S(5) lines are presented. The H₂S(0) and H₂S(1) lines (figure 1) lie in the LL module of the IRS and the resolution of the maps is 5.08 arcsec. The H₂S(2) - H₂S(5) lines (figure 2) lie in the SL module of the IRS and these maps each have a resolution of 1.85 arcsec. This explains the relative smoothness of H₂S(0) and H₂S(1) maps compared to the H₂S(2) - H₂S(5) maps. The boxes around the maps represent the regions over which the lines were mapped.

Maps reveal remarkable differences in the morphology of NGC 5194. H₂S(0) emission is strongest in the NW spiral arm with much lower levels of emission coming from the nucleus. The H₂S(1) emission peaks in the nucleus of the galaxy with strong emission in the NW and SE spiral arms. In the H₂S(0) and H₂S(1) emission, we are able to resolve molecular hydrogen emission in the outer spiral arms at several kiloparsecs from the center of the galaxy. While we have resolved molecular hydrogen emission in the outer spiral arms, the peaks in H₂S(0) and H₂S(1) emission within the arms do not align.

The higher resolution H₂S(2) - H₂S(5) maps also show different morphology to NGC 5194. The H₂S(2) map shows the strongest emission in the nuclear region of NGC 5194. The H₂S(3) line exhibits similar strong emission in the nuclear region; however, there appears to be a bar structure across the nucleus of the galaxy going north-to-south. Again, we see offsets in the peak emission within the spiral arms of NGC 5194. These offsets are real and indicate variations in the excitation-temperature in each region.

Maps of the H₂S(4) and H₂S(5) lines show a remarkably different morphology to the nuclear region of NGC 5194. The H₂S(5) nuclear emission follows the nuclear emission of the H₂S(3) line, while the H₂S(4) nuclear emission mirrors the H₂S(2) emission. This indicates variations in the excitation-temperature (further explored in section §3.3).

Due to the sensitivity of the IRS low resolution module, we were unable to resolve H₂S(4) and H₂S(5) emission beyond the central region of NGC 5194. For the same reason, we were unable to create maps of the H₂S(6) (at 6.11 μ m) and H₂S(7) (at 5.51 μ m) lines. Deeper observations could reveal more complete maps of the H₂S(4) and H₂S(5) emission in NGC 5194 in addition to allowing us to map the H₂S(6) and H₂S(7) lines across NGC 5194.

3.2. Mapping H₂ Excitation-Temperature and Mass

The pure rotational lines of molecular hydrogen provide a powerful probe of the conditions of the ISM and place constraints on the energy injection processes that excite H₂. Knowledge of the extinction corrected flux of the H₂S(0) - H₂S(5) lines allow for the mapping of the excitation-temperature and number density (and consequently mass). The excitation-temperature and mass can be modeled across the galaxy by creating excitation diagrams at every position across the strip of NGC 5194.

Excitation diagrams across NGC 5194 were created from the maps of H₂ emission. Each map was smoothed and interpolated to the resolution of the H₂ S(0) line. The non-rectangular shape to the excitation-temperature and mass are due to the offset in alignment between the LL and SL strips. Excitation diagrams across the strip were derived from the Boltzman equation in similar form to the Rigopoulou et al. (2002).

$$N_i/N = (g(i)/Z(T_{\text{ex}})) \exp(-T_i/T_{\text{ex}}) \quad (1)$$

where $g(i)$ is the statistical weight of state i , $Z(T_{\text{ex}})$ is the partition function, T_i is the energy level of a given state, and T_{ex} is the excitation temperature. N and N_i are the total column density and the column density of a given state i and is determined directly from the measured extinction corrected flux by

$$N_i = \text{flux}(i)/(A(i)h\nu(i)) \quad (2)$$

where $A(i)$ and $\nu(i)$ are the A-coefficient and frequency of state i and h is Planck's constant. Table 1 lists the values for the wavelength ($\lambda(i)$), rotational state (J), $A(i)$, T_i , and $g(i)$ of the pure rotational levels of H₂ that lie in the wavelength range covered by the IRS low resolution modules.

The excitation diagrams exhibit an ortho-to-para ratio (OPR) in the nuclear region 3 (in agreement with the value of the OPR of the nuclear region determined by SINGS

(Roussel et al. 2007, in press); this is determined from the fit to the best two-component fit to the H₂S(0) - H₂ S(5) lines. Outside of the nuclear region, poor detection of the H₂ S(4) and H₂ S(5) lines prevents the mapping of OPR across the disk; however, the lower J lines exhibit an OPR of 3 within the spiral arms.

In the nuclear region of NGC 5194, the excitation diagram is smooth and its slope decreases at higher rotational levels (Figure 3). This indicates that there is a range of temperatures being sampled within the beam. Similar behavior has been observed in extragalactic targets by surveys of Seyferts (Rigopoulou et al. 2002) and ULIRGS (Higdon et al. 2006). The temperature of the warm ($T = 100 - 300$ K) H₂ and the temperature of the hot ($T = 400 - 1200$ K) H₂ can be determined from the excitation diagrams by fitting the H₂S(0) - H₂S(2) lines and the H₂S(2) - H₂S(5) lines respectively (as opposed to fitting all of the observed H₂ rotational lines in order to derive a temperature of the warm H₂).

From a two-component fit to the excitation diagram, the excitation-temperature of the “warm” and “hot” components of H₂, the “warm” and “hot” H₂ mass have been mapped across NGC 5194 (figures 4, 5, and 6). In measuring the mass in H₂, we determine the mass from the number density by multiplying the column density by the physical area within the beam (Rigopoulou et al. 2002). At 9.6 Mpc (Sandage and Tammann 1975), 5.08 arcsec corresponds to 236.43 parsecs. The maps of the mass distribution are in units of solar masses within a 55.899 kpc² region.

Figure 4 compares the warm H₂ mass to the temperature distribution of the mass. The gas is warmest in the central region of NGC 5194 with the temperature ranging from 225K - 275 K in the center of the galaxy. The gas is coolest within the spiral arms of NGC 5194. The outer NW and SE spiral arms (at about 6-7 kpc from the center of the galaxy each) contain on the order of 10,000 M_⊙ (within a 55.9 kpc² region) and 6,000 M_⊙ (within a 55.9 kpc² region) of H₂ (in the NW and SE arms, respectively) and the gas within

the outer spiral arms ranges from 150 K at the center of the arms to about 225 K near the edges. Within the central 0.000 pc^2 of the galaxy, there is $0.000 M_\odot$ of warm H_2 and $0.00000 M_\odot$ hot H_2 . These values are consistent with the masses of H_2 found in the central regions of Seyferts (Rigopoulou et al. 2002). In NGC 5194, the IRS is sensitive to $375 M_\odot$ warm H_2 and $5 M_\odot$ hot H_2 within the beam (though the sensitivity to the hot H_2 could be underestimated due to smoothing the $\text{H}_2\text{S}(2)$, $\text{H}_2\text{S}(3)$, $\text{H}_2\text{S}(4)$, and $\text{H}_2\text{S}(5)$ lines by a factor of 3 times their resolution).

Note that due to zero detection of H_2 in some of the inner arm regions, we are unable to determine the temperature distribution across the entire strip. This is evident towards the NW and SE edges of the radial strip.

The temperature and mass distribution of the hot H_2 reveals a different picture (Figure 5). There is significantly less mass in the hot H_2 phase, on the order several hundred M_\odot , depending on the region. The greatest amount of hot H_2 is found within the nuclear region of NGC 5194; this is much different from the warm H_2 that dominates the spiral arms. The hot gas exhibits cooler temperatures within the central regions of NGC 5194 and the spiral arms. Temperatures are greater in the inter-arm regions where there is less H_2 .

Due to the weakness of the $\text{H}_2\text{S}(2)$, $\text{H}_2\text{S}(3)$, $\text{H}_2\text{S}(4)$, and $\text{H}_2\text{S}(5)$ features beyond the spiral arms, the hot H_2 excitation temperature and mass can not be mapped over the whole strip. While the radial strip across NGC 5194 is helpful in understanding the H_2 excitation-temperature and mass across the disk of the galaxy, complete IRS low resolution coverage of NGC 5194 with longer integration time is necessary in order to understand hot H_2 distribution and the H_2 OPR across the whole galaxy.

4. Discussion

4.1. Distinguishing the H₂ Excitation Mechanisms

Previous studies of pure rotational H₂ emission in galaxies have used aperture average spectra over the central regions of galaxies to understand the distribution of the warm and hot molecular gas phases within a galaxy (Rigopoulou et al. 2002, Higdon et al. 2006, Roussel et al. 2007, in press). These studies use the pure rotational lines to derive excitation-temperatures and warm and hot H₂ masses of the H₂ within the galaxy. Additionally, these studies compare the warm and hot H₂ mass to the cold H₂ mass traced by CO emission to in order to understand the mass fractions of the cold ($T = 5 - 10$ K), warm, and hot H₂ mass. These studies have had difficulty distinguishing the H₂ excitation mechanisms within the galaxies

H₂ is generally excited via three processes: 1.) excitation in photodissociation regions (PDRs) , 2.) shocks, and 3.)x-ray dissociation (XDRs). Mapping the warm and hot H₂ mass-excitation temperature and mass distributions provide the information necessary to understand whether the warm and hot H₂ phases undergo excitation via the same mechanism. This information coupled with spatially resolved diagnostics of PDRs, shocks, and XDRs put constraints on the dominant H₂ excitation mechanism in NGC 5194, in different regions within NGC 5194.

Figure (??) compares the warm H₂ excitation temperature distribution to the mass distribution. The excitation temperature is greatest within the nuclear region of the galaxy and is cooler in the spiral arms. Within the nuclear region, the excitation temperature decreases moving radially away from the center of the galaxy. Moving into the inner spiral arms, the excitation temperature decreases. The excitation temperature within the inter-arm regions is greater than in the spiral arms.

The excitation-temperature for the hot H₂ phase peaks in the inter-arm regions (figure ??); the hot H₂ mass peaks in the nuclear region of the galaxy. This is contrasted to the warm H₂ mass that peaks in the SW spiral arm. Directly comparing the warm H₂ mass to the hot H₂ mass, shows that the ratio of warm-to-hot H₂ is greater in spiral arms than in the nuclear region of the galaxy (figure ??). In the nuclear region of the galaxy, the ratio of warm-to-hot H₂ is 100. Moving into the NW inner spiral arm and SE inner spiral arm, the ratio increase by a factor of 8 and 6.5 respectively.

The variations of the warm-to-hot mass ratio across the strip over NGC 5194 indicates that the primary excitation mechanisms of the warm and hot H₂ differ. The warm H₂ mass peaks in the NW inner spiral arm whereas the hot H₂ mass peaks in the center. This suggests that the warm H₂ is associated with giant molecular clouds within spiral arms and is primarily excited by PDRs. NGC 5194 is known to host a weak AGN in its nucleus (citation). The hot H₂ mass peaks in the nuclear region. This could mean that the warm phase is primarily excited by the AGN.

In order to understand the excitation mechanisms of the warm H₂ and the hot H₂ and where each is dominant, we present comparisons of the H₂ mass distributions to diagnostics of the three excitation mechanisms (PDRs, shocks, and XDRs). CO rotational transitions are used as diagnostic lines of PDRs (Allen et al., 2004). Comparing the H₂ mass distributions to CO ($J = 1 - 0$) thus compares the location of the H₂ mass to locations of giant molecular clouds. The [OIV](25.98 μm) emission arises fro shocks (Schaerer and Stasinska 1999). Spatial mapping of [OIV](25.89 μm) emission thus serves to discern regions where H₂ is excited primarily by shocks. H₂ excitation by x-rays can also be discerned within M51a by comparing the H₂ mass phases and emission to x-ray emission observed by the Chandra X-ray Observatory (Terashima and Wilson 2001). The following sections compare the H₂ mass distributions to CO ($J = 1 - 0$) emission, [OIV](25.89 μm) emission,

and x-ray emission.

4.2. H₂ Excitation by PDRs: Comparison of H₂ to CO emission

While massive amounts of molecular gas have been observed at higher resolution within the nucleus of NGC 5194 (Scoville et al. 1998); the majority of the warm H₂ is found in the spiral arms indicating the photodissociation by UV photons from giant molecular clouds is the primary mechanism for exciting the warm H₂ phase.

4.3. H₂ Excitation by Shocks: Comparison of H₂ to [OIV](25.89 μ m) emission

The [OIV](25.89 μ m) line can be excited in shocks, the stellar winds of massive Wolf-Rayet stars, or by a active galactic nucleus (AGN)(Schaerer and Stasinska 1999, Lutz et al. 1998, Smtih et al. 2004). Though the [OIV](25.89 μ m) line is bledened with the [FeII](25.99 μ m) line in Spitzer IRS low resolution spectra; however, PAHFIT can deblend the two lines. Thus, in mapping the H₂ S(0) and H₂ S(1) line in the LL data cubes, [OIV](25.89 μ m) emission is also be mapped. Figure (??) compares the [OIV](25.89 μ m) emission to the hot H₂ disribution. The [OIV] emission is brightest in the central region of the galaxy and its peak is cospatial with the peak in the mass of the hot H₂. Moving from the nucleus to the inner spiral arm, the [OIV](25.89 μ m) emission subsides. Note also weak [OIV] emission within the spiral hot H₂ spiral arms and in the inter-arm region (toward the SE spiral arm).

The [OIV](25.89 μ m) emission within the nuclear region is likely due to the weak Seyfert 2 nucleus (Ford et al. 1985) and could possibly be associated with shocked gas from the outflows of the AGN. The peak of the [OIV](25.89 μ m) emission coincides with the peak in hot H₂ mass indicating that the hot H₂ phase in the nuclear region of the galaxy

is AGN or shock heated. With about $1000 M_{\odot}$ of hot H₂ in the central 0.5 kpc², it is unlikely that the hot H₂ is fueling the central AGN, but rather is excited by the AGN or shocks produced by it. While the warm H₂ mass does not peak in the nuclear region of the galaxy, there is still a factor of $\geq 100 M_{\odot}$ of H₂ in the inner .05 kpc². In fact, strong nuclear [OIV](25.89 μ m) emission is not cospatial with the warm ($T = 100 - 300$ K) H₂ distribution indicating that AGN heating or shocks are not the primary mechanism for exciting H₂ in the nuclear region.

Comparing the [OIV](25.89 μ m) emission to the warm ($T = 100 - 300$ K) H₂ reveals that the [OIV] (25.89 μ m) emission to the inner edge of the inner spiral arms. The [OIV](25.89 μ m) emission decreases in strength across the spiral arm.

4.4. H₂ Excitation by XDRs: Comparison of H₂ to X-ray emission

M51 has been extensively studied in x-rays by ASCA (Terashima et al. 1998), Newton XMM (Dewangen et al. 2005), and the Chandra X-ray Observatory (Terashima and Wilson 2001). These observations of the M51a,b system have revealed more than 80 x-ray sources. Candidates for these x-ray sources include neutron stars, black holes, supernova remnants (SN 1994I), and a low-luminosity AGN (Terashima et al. 2006, Immler et al. 2002, Terashima and Wilson 2001). X-ray emission from the nuclear region of NGC 5194 has been studied by Terashima and Wilson (2001). At 1" resolution, they observe x-ray emission from the nucleus, an extranuclear cloud (XNC, to the south of the nucleus), and the northern loop. A radio jet has been observed connecting the nucleus of NGC 5194 to the XNC in 6 cm imagery (Crane and van der Hulst 1992). The jet emanates from the south of the elongated nucleus and is shock heating ISM.

Figure (?) compares the 0.5 - 10 keV x-ray band image to the warm and hot H₂ mass

distributions. There is very little correlation between the 0.5 - 10 keV x-ray emission and the warm H₂ mass distribution indicating that x-rays play very little role in heating the warm H₂ mass. X-ray emission does correlate with the hot H₂ mass. The brightest 0.5 - 10 keV x-ray emission originates from the nucleus and the southern XNC. The hot H₂ mass peak is cospatial with the nucleus and the mass decreases into the XNC. Additionally, the hot H₂ mass decreases moving into the northern loop. The correlation between x-ray emission from the nucleus of NGC 5194 and the peak in hot H₂ mass suggests that x-rays play an important role in exciting the hot phase of H₂; however, due to the disparity in resolution between the x-ray image and the H₂ maps (1" resolution for x-rays 5".08 resolution for the warm and hot H₂ mass) it is difficult to distinguish between shock excitation and x-ray excitation of H₂ in the nuclear region of NGC 5194.

In order to distinguish between shock excitation and x-ray excitation of H₂ in the nuclear region of NGC 5194, we compare the x-ray emission to the maps of the higher *J* H₂ emission maps. These maps have a resolution of 1".85. The H₂ S(3) and H₂ S(5) emission both are strongest between the nucleus and XNC, at the location of the radio jet, with the emission decreasing moving south into the XNC. The strength of the H₂ S(3) and H₂ S(5) lines also decreases across the nucleus and into the northern spiral arm; however, the gradient is less steep. The map of H₂ S(3) emission shows that the bar structure in H₂ emission is aligned with the AGN, radio jet, XNC, and northern loop. The peak in H₂ S(2) emission is centered on the nucleus and radio jet with the emission decreasing by 60% across the XNC.

The offset of the peak in H₂ S(2), H₂ S(3), and H₂ S(5) emission to the south the nucleus at the location of the jet indicates that the lower *J* H₂ lines are being shock heated by the radio jet in NGC 5194.

5. Conclusions

We have mapped the pure rotational H₂ emission over NGC 5194 using the Spitzer IRS low resolution modules. We have used maps of the H₂ emission to understand the spatial distribution of warm ($T = 100 - 300$ K) and hot ($T = 400 - 1000$ K) H₂ in NGC 5194. We find:

1. The morphology of H₂ emission in NGC 5194 varies with H₂ rotational level. H₂ S(0) emission is strongest in the spiral arms of the galaxy while the lower J transitions show the strongest emission towards the nucleus. The H₂ S(0) and H₂ S(1) maps (at 5.08 arcsec resolution) show emission across the entire strip out to spiral arms located several kpc from the center of the galaxy. The H₂ S(2) and H₂ S(3) maps (at 1.85 arcsec resolution) reveal H₂ in the nucleus, spiral arms, and inter-arm regions of NGC 5194. An interesting example is that H₂ S(3) emission reveals bar structure across the center of the galaxy. Strong H₂ S(4) and H₂ S(5) emission is resolved in the nuclear region of NGC 5194.
2. The different morphologies of H₂ emission in NGC 5194 indicate variations in H₂ excitation-temperature, mass, and OPR. From maps of the emission of the lowest pure rotational transitions, the excitation-temperature and mass are mapped across the strip. The excitation-temperatures of the warm and hot phases are higher in the nucleus and inter-arm regions of the galaxy and lower in the spiral arms. We find that the warm H₂ and the hot H₂ are not cospatial. The hot mass peaks in the central region of NGC 5194 and the warm mass peaks in the NW spiral arm (in our strip coverage). Ratio maps indicate the the warm-to-hot mass ratio varies in NGC 5194. In the nucleus, the ratio is 100 and it increases to 800 in the NW spiral arm. Variations in the warm-to-hot H₂ ratio indicate that the primary excitation mechanism differs between warm and hot H₂.
3. We compare the warm and hot H₂ to the cold H₂ traced by CO ($J = 1 - 0$) emission.

The largest amounts of cold and warm H₂ are found in the spiral arms while the

4. The NGC 5194 is a Seyfert II galaxy that hosts a weak AGN in its nucleus. We observe strong [OIV](25.89 μm) emission from the central region of the galaxy. The [OIV](25.89 μm) emission is cospacial with the hot H₂ mass suggesting that the hot H₂ is primarily excited by an AGN or by strong shocks (possibly associated with the central AGN). It should be noted that x-ray excitation can not be excluded as an excitation mechanism for the hot H₂. Strong x-ray emission has been observed in from the central AGN in NGC 5194

The author acknowledges the support of Spitzer Science Center and the Spitzer Visiting Graduate Student Fellowship Program for providing support for this research. The author would also like to thank JD Smith for swift responses to questions about PAHFIT and CUBISM and Nicolas Flagey for productive discussions about PAHFIT.

Facilities: Spitzer Science Center (SSC), Spitzer Space Telescope (SST), Berkely-Illinois-Maryland Array (BIMA).

REFERENCES

- Aalto et al., 1999, AJ, 522, 165
- Allen, R.J., Heaton, H.I., and Kaufman M.J., 2004, ApJ, 608, 314
- Bloemen et al., 1986, A&A, 154, 25
- Calzetti et al., 2005, ApJ, 633, 871
- Crane, P.C. and van der Hulst, J.M., 1992, AJ, 103, 1146
- Dewangn, G.C., Griffiths, R.E., Choudhury, M., Miyaji, T., and Schurch, N.J., 2005, ApJ, 635, 198
- Ford, H.C., Crane, P.C., Jacoby, G.H., Lawrie, D.G., and van der Hulst, J.M., 1985, ApJ, 293, 132
- Fuente et al., 1999, ApJ, 518, L45
- Helfer, Thornley, Regan, Wong, Sheth, Vogel, Blitz, and Bock, 2003, ApJS, 145, 259
- Higdon et al., 2006, ApJ, 648, 323
- Houck et al., 2004, ApJS, 145, 18
- Immler, S., Wilson, A.S., and Terashima, Y., 2002, ApJ, 573, L27
- Kaufman, Wolfire, and Hollenbach, 2006, ApJ, 644, 283
- Lutz et al., 1998, AA, 333, L75
- Kennicutt et al., 2003, PASP, 115, 928
- Matsushita et al., 2004, ApJ, 616, L55

Murphy et al., 2006, ApJ, 638, 157

Neufeld, Melnick, and Harwit, 1998, ApJ506, L75

Neufeld, Melnich, Sonnentrucker, Bergin, Green, Kim, Watson, Forrest, and Pipher, 2006,
ApJ, 649, 816

Palumbo, Fabbiano, Franson, and Trinchieri, 1985, ApJ, 298, 259

Regan, Thornley, Helfer, Sheth, Wong, Vogel, Blitz, and Bock, 2001, ApJ, 561, 218

Rigopoulou et al., 2002, A&A, 389, 374

Rodriguez-Fernandez, Martin-Pintado, de Vicente, Fuente, Huttmeister, Wilson, and
Kunze, 2000, A&A, 356, 695

Roussel et al., 2007, TBD

Ridbeck et al., 1985, A&A, 144, 282

Sandage and Tammann, 1975,

Schaerer, D. and Stasinska, G., 1999, A&A, 345, L17

Scoville, N.Z. and Young, J.S., 1983, AJ, 265, 148

Scoville, N.Z., Yun, M.S., Armus, L., and Ford, H., 1998, ApJ, 493, L63

Scoville et al., 2001, AJ, 122, 3017

Sheth et al., 2000, ApJ, 532, 221

Sheth, Vogel, Regan, Thornley, and Teuben, 2005, ApJ, 632, 217

Smith et al., 2004, ApJS, 154, 199

Smith, Armus, Buckalew, Dale, Helou, Roussel, and Sheth, 2006, CUBISM User Manual

Smith et al., 2007, ApJ, accepted

Smith et al., 2007, in preparation

Sternberg and Neufeld, 1999, ApJ, 516, 371

Takahashi, 2001, ApJ, 561, 254

Terashima, Y., Ptak, A., Fujimoto, M.I., Kunieda, H., Makishima, K., and Sherlemitsos, P.J., 1998, ApJ, 496, 210

Terashima and Wilson, 2001, ApJ, 560, 139

Timmermann et al., 1996, A&A, 315, L281

Timmermann, 1998, ApJ, 498, 246

Valentijn et al., 1996, A&A, 315, L145

Vogel, Kulkarni, and Scoville, 1988, Nature, 334, 402

Terashima, Y. and Wilson, A.S., 2001, ApJ, 560, 139

Wright et al., 1996, A&A, 315, L301

Young and Deveraux, 1991, ApJ, 373, 414

Young, J.S. and Scoville, N.Z., 1991, ARA&A, 29, 581

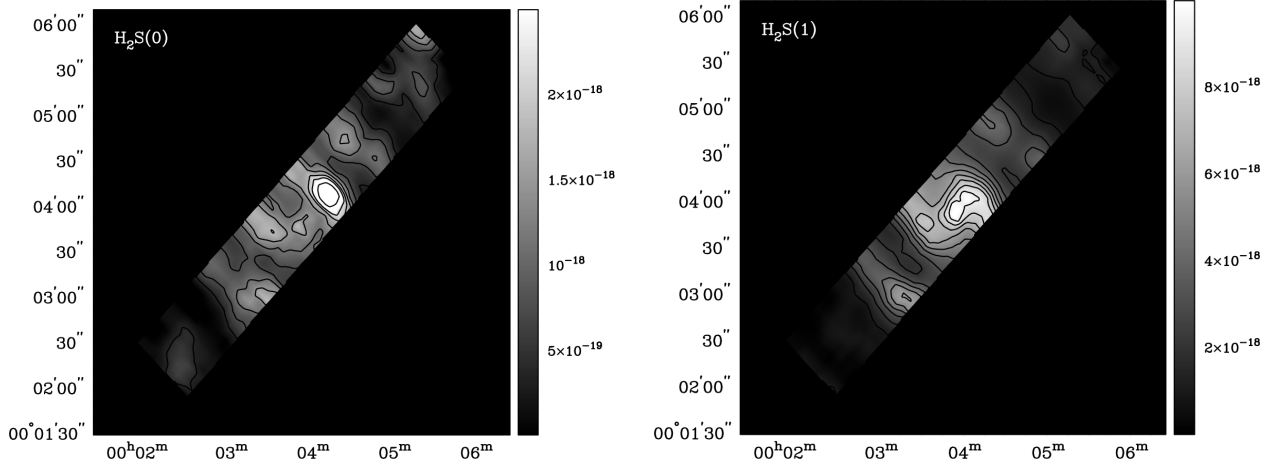


Fig. 1.— H₂S(0) (left) and H₂S(1) (right) emission across the IRS LL radial strip is shown. Maps are in units of W/m². Contour levels are at 2.9×10^{-18} , 2.2×10^{-18} , 1.8×10^{-18} , 1.5×10^{-18} , 1.1×10^{-18} , 7.3×10^{-19} , and 3.7×10^{-19} W/m² for H₂S(0); 9.6×10^{-18} , 8.6×10^{-18} , 7.5×10^{-18} , 6.4×10^{-18} , 5.4×10^{-18} , 4.3×10^{-18} , 3.2×10^{-18} , 2.1×10^{-18} and 1.1×10^{-18} W/m² for H₂S(1). The resolution of both maps is 5.08 arcsec. Note that in all of the maps, north is up and west is to the left.

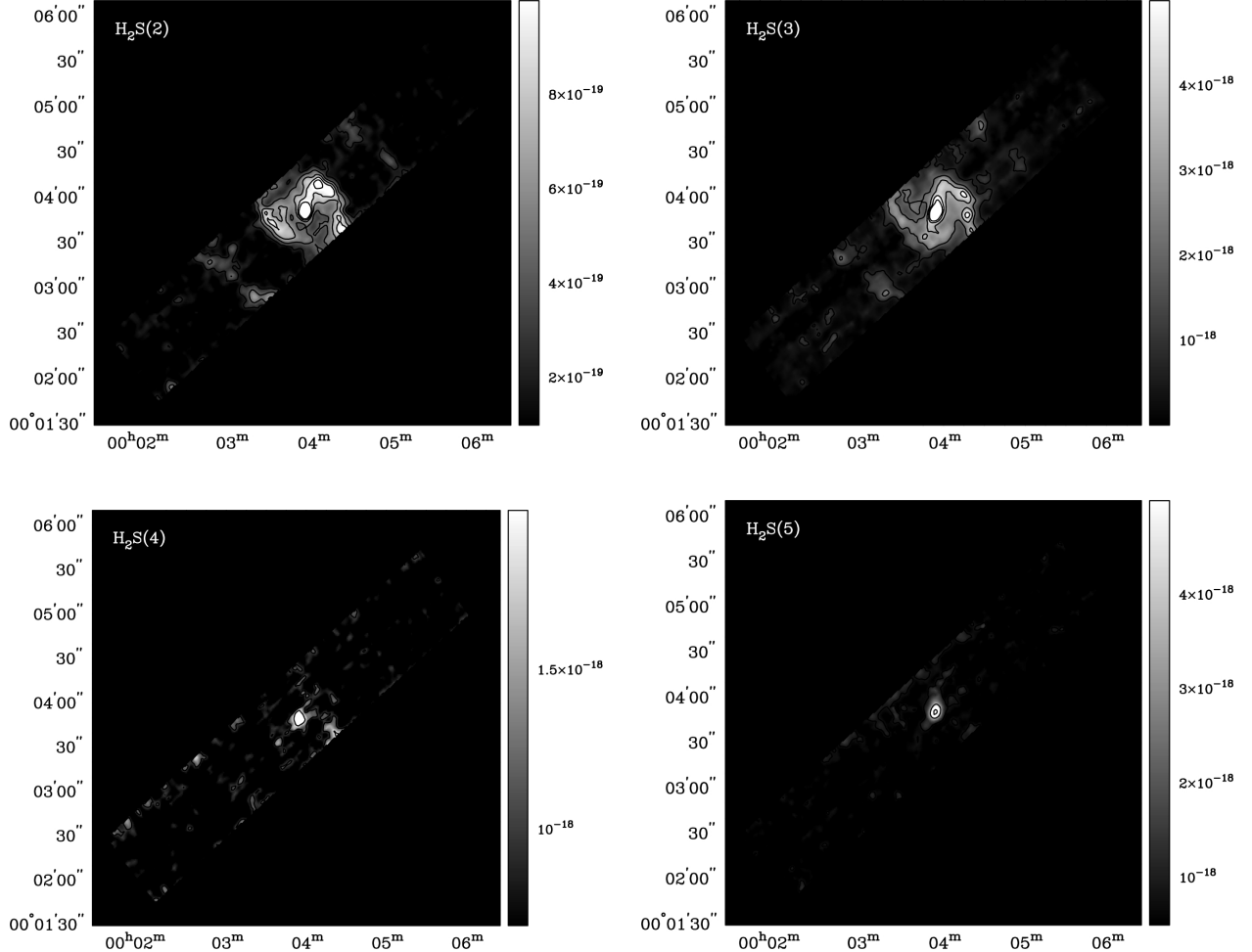


Fig. 2.— Maps of H₂ S(2) (top left), H₂ S(3) (top right), H₂ S(4) (bottom left), and H₂ S(5) (bottom right) emission across the IRS SL radial strip are shown. Maps are in units of W/m². Contours levels are at 1.1×10^{-18} , 8.9×10^{-19} , 6.7×10^{-19} , 4.4×10^{-19} , and 2.2×10^{-19} W/m² for H₂ S(2); 1.21×10^{-17} , 9.4×10^{-18} , 6.7×10^{-18} , 4.0×10^{-18} , and 1.3×10^{-18} W/m² for H₂ S(3); 2.0×10^{-18} and 1.0×10^{-18} W/m² for H₂ S(4); 7.3×10^{-18} , 4.0×10^{-18} , and 8.0×10^{-19} W/m² for H₂ S(5). The resolution of all four maps is 1.85 arcsec.

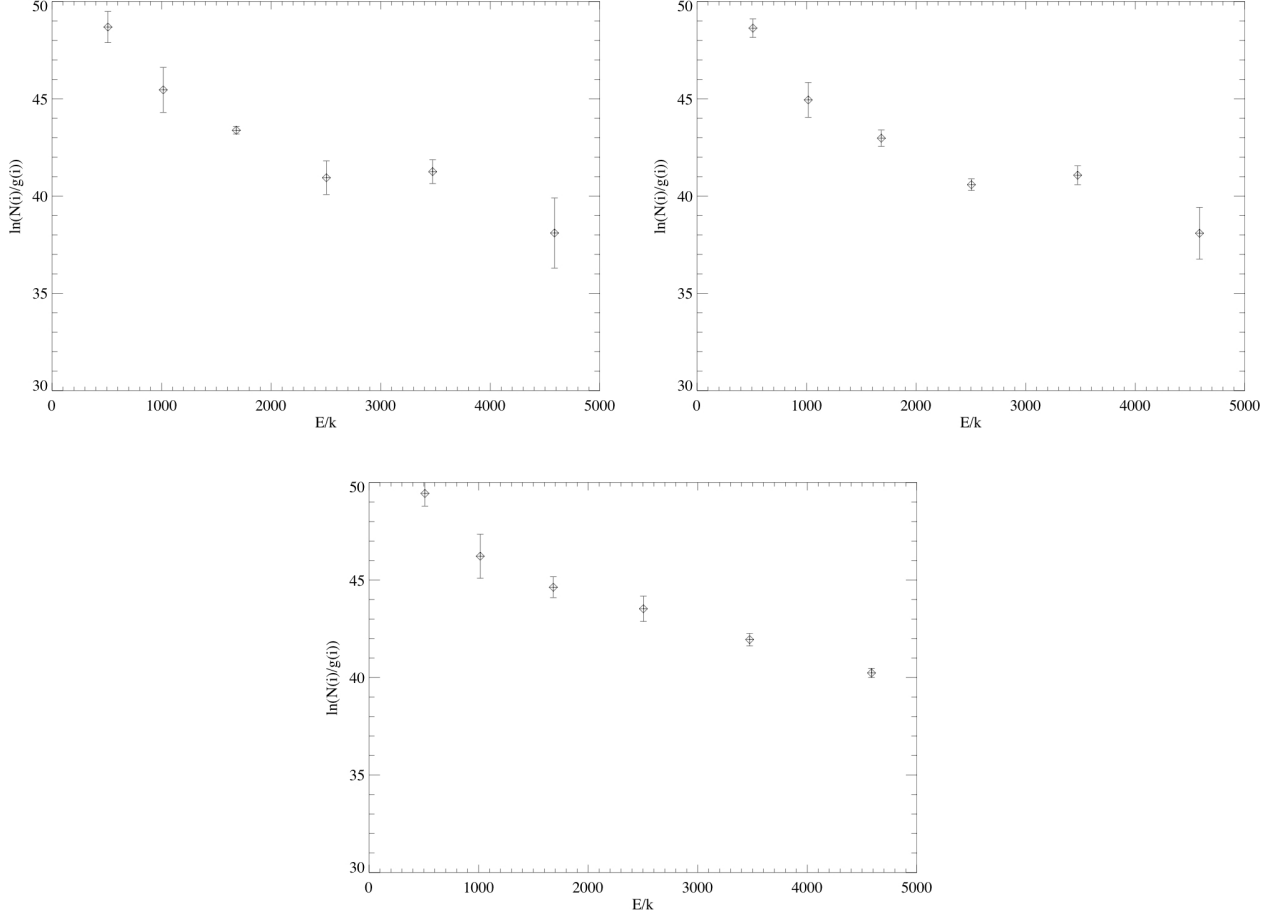


Fig. 3.— Sample excitation diagrams taken from different regions along the NGC 5194 strip. The top two excitation diagrams are taken from the different spiral arms at 25 arcsec^2 regions at (RA, Dec) of (202.45, 47.21) and (202.49, 47.18), respectively. The excitation diagram at the bottom is taken from a 25 arcsec^2 region in the center of NGC 5194 at (RA, Dec) of (202.47, 47.19).

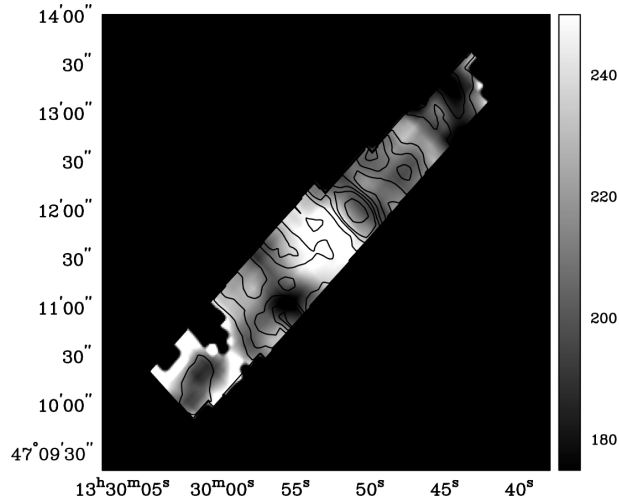


Fig. 4.— The warm ($T = 175 - 250$ K) H_2 mass compared to the warm H_2 temperature distribution. Mass contour levels are at 10% of the maximum mass ($3.10 \times 10^4 M_\odot$). Contours represent the mass within a 55.9 kpc^2 area.

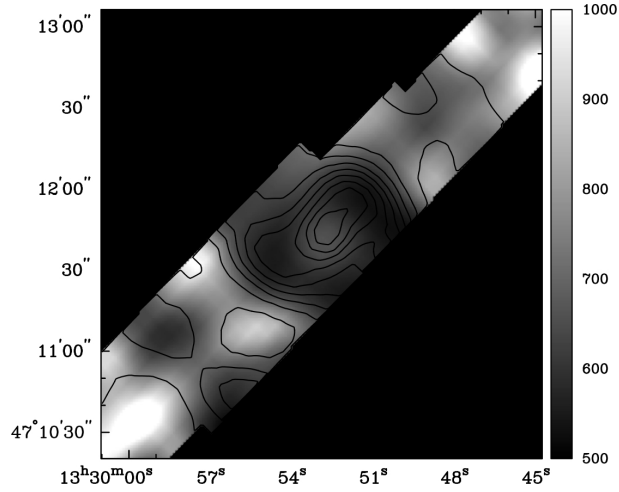


Fig. 5.— The hot ($T = 500 - 1000$ K) H_2 mass compared to the hot H_2 temperature distribution. Mass contour levels are at 10% of the maximum mass ($92.5 M_\odot$). Contours represent the amount of mass of the hot H_2 within a 55.9 kpc^2 area.

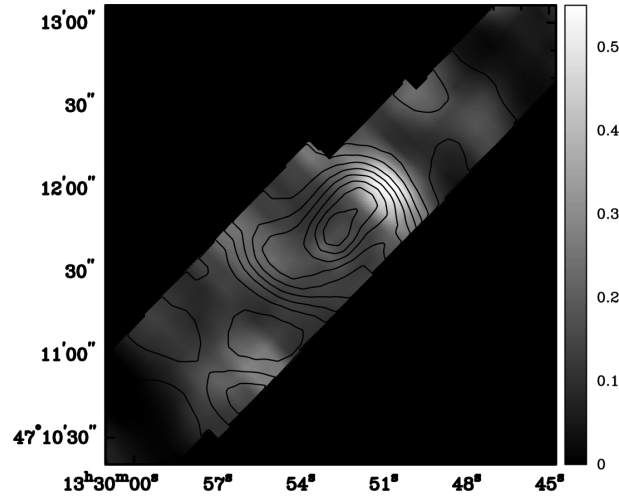


Fig. 6.— The warm (175K - 250 K) H₂ mass (represented by the map) compared to the hot (T = 500 - 1000 K) H₂ mass (in contours).

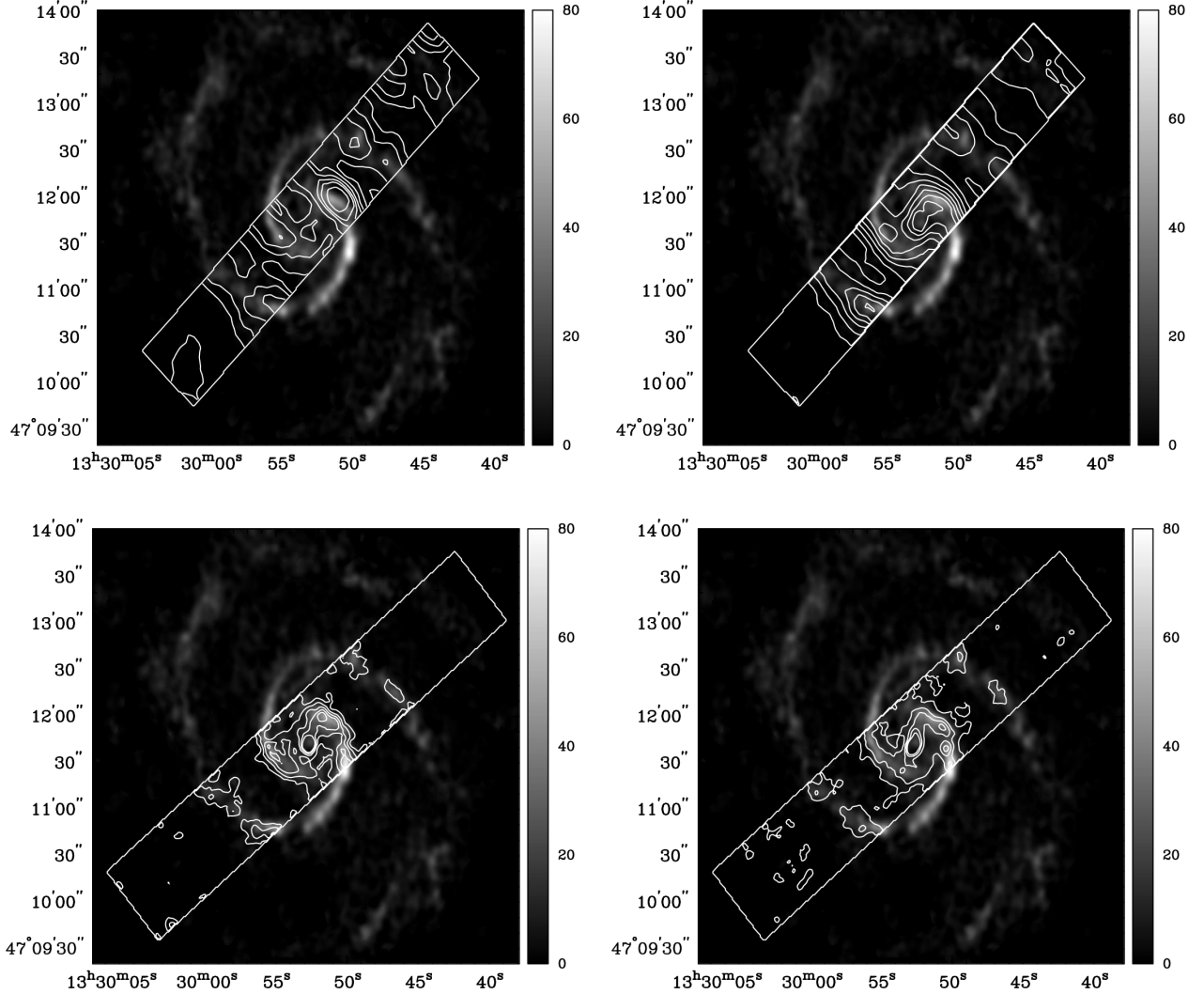


Fig. 7.— Comparison of the CO emission to the H₂S(0) (top left), H₂S(1) (top right), H₂S(2) (bottom left), and H₂S(3) (bottom right) emission. The CO emission maps are in units of Jy beam s⁻¹. Contour levels for H₂S(0), H₂S(1), H₂S(2), and H₂S(3) are at the same levels as those used in figures 1 and 2.

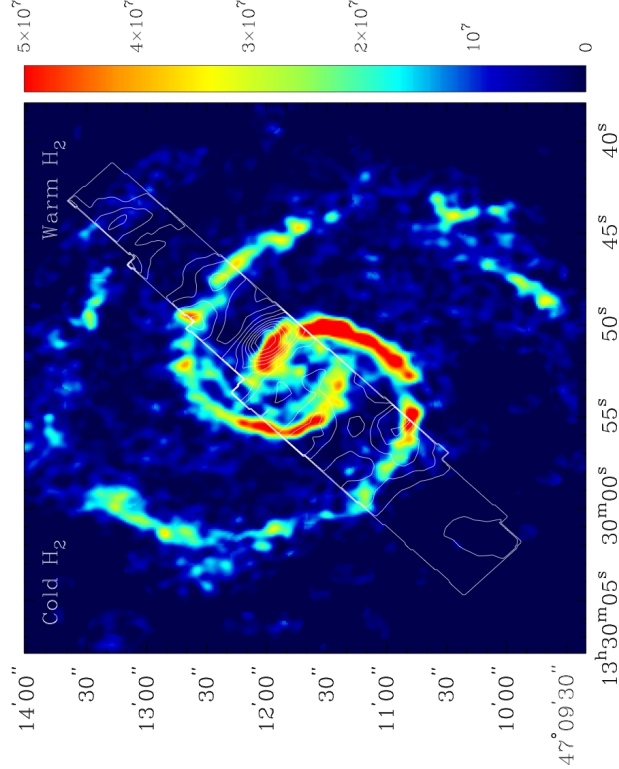


Fig. 8.— Comparison of the cold H₂ (as traced by the CO emission) to the warm (T = 150-250 K) H₂ mass. Cold H₂ mass is in units of M_⊙. Warm H₂ mass contours are the same as in Figure 4.

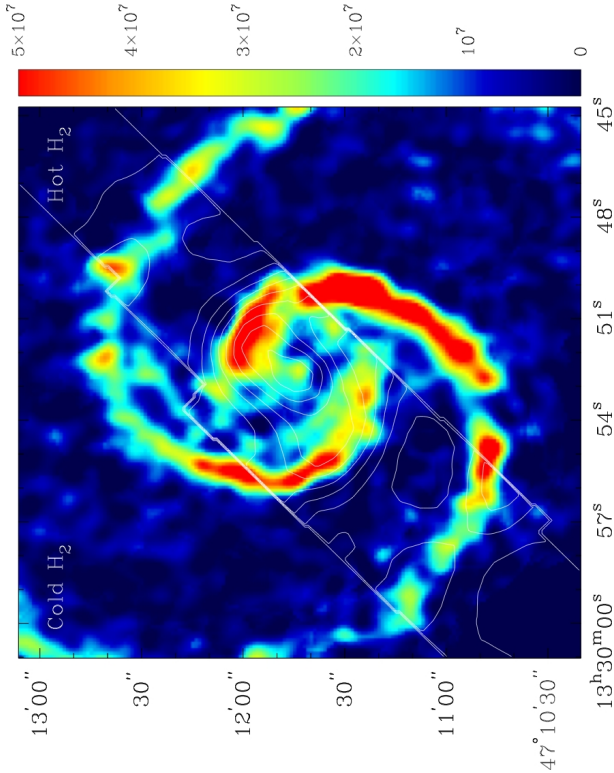


Fig. 9.— Comparison of the cold H₂ (as traced by CO emission) to the hot (T = 500-1000 K) H₂ mass. Cold H₂ mass is in units of M_⊙. Hot H₂ mass contours are the same as in Figure 5.

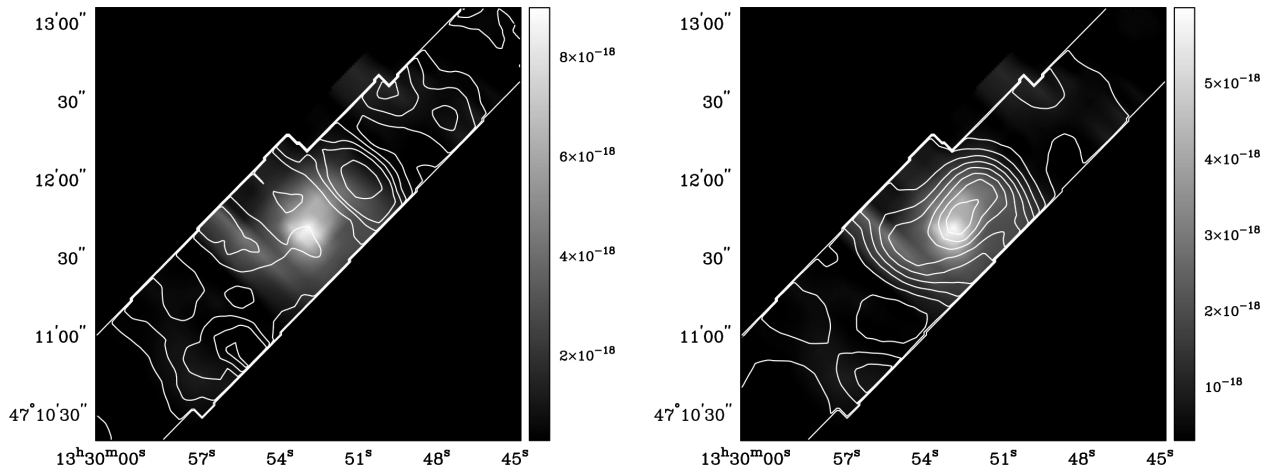


Fig. 10.— *Left:* Comparison of the [OIV](25.89 μ m) emission to the warm ($T = 100$ K - 300 K) H₂ mass distribution. Hot H₂ mass contours are the same as in Figure 4. *Right:* Comparison of the [OIV](25.89 μ m) emission to the hot ($T = 400$ - 1000 K) H₂ mass distribution. Hot H₂ mass contours are the same as in Figure 5. The [OIV](25.89 μ m) emission is in units of W/m².

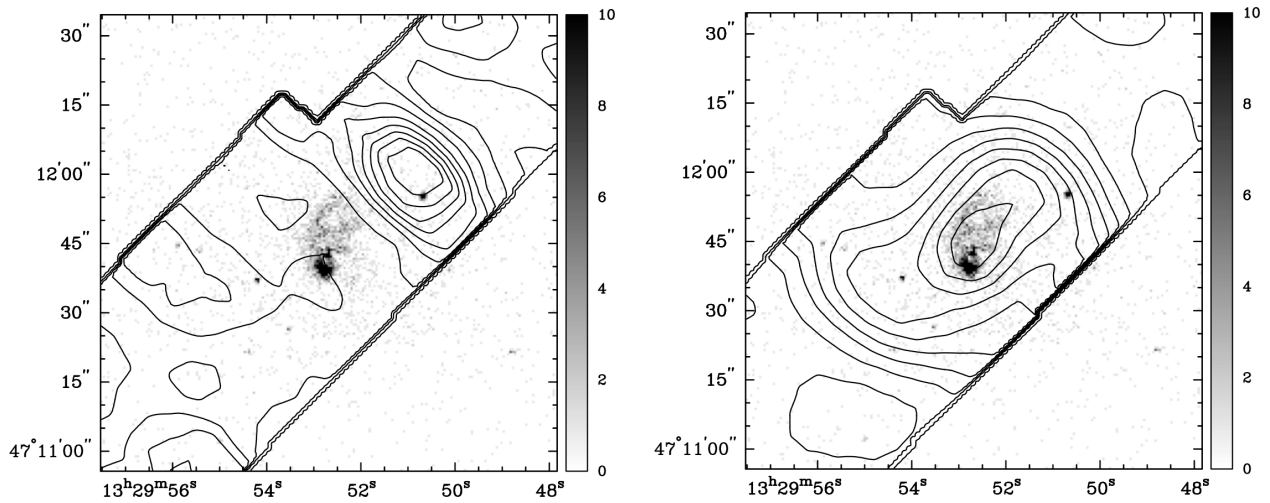


Fig. 11.— *Left:* Comparison of the 0.5 - 10 keV x-ray emission band to the warm ($T = 175$ - 250 K) H_2 mass distribution. X-ray emission is in units of counts. H_2 mass contours are the same as in figure 4. *Right:* Comparison of the 0.5 - 10 keV x-ray emission band to the hot ($T = 500$ - 1000 K) H_2 mass distribution. The H_2 mass distribution contours are the same as in figure 5.

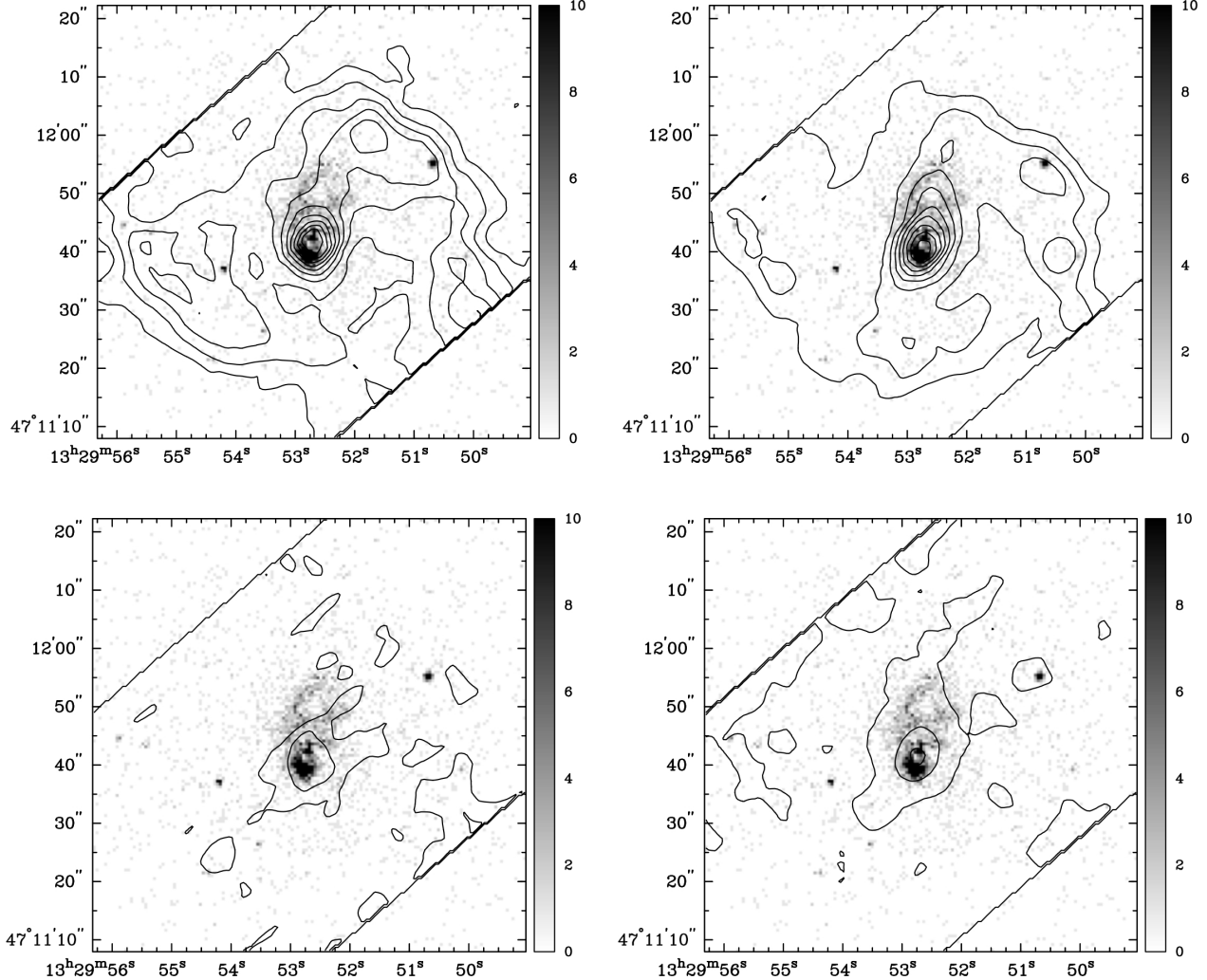


Fig. 12.— Comparison of 0.5 - 10 keV x-ray emission band to the H₂ S(2) (top left), H₂ S(3) (top right), H₂ S(4) (bottom left), and H₂ S(5) (bottom right) emission in the nuclear region of NGC 5194. X-ray emission is in units of counts. The H₂ S(2) and H₂ S(3) emission contours are at 10% of their peak values (2.20×10^{-18} and $1.35 \times 10^{-17} \text{ W/m}^2$, respectively). The H₂ S(4) contours are at 2.0×10^{-18} and $1.0 \times 10^{-18} \text{ W/m}^2$ and the H₂ S(5) contours are at 7.3×10^{-18} , 4.0×10^{-18} , and $8.0 \times 10^{-19} \text{ W/m}^2$.

Table 1. H₂ Parameters

Transition	Wavelength (μm)	Rotational State (J)	Energy (E/k)	A (s^{-1})	Statistical Weight (g)
H ₂ (0-0)S(0)	28.22	2	510	2.94x10 ⁻¹¹	5
H ₂ (0-0)S(1)	17.04	3	1015	4.76x10 ⁻¹⁰	21
H ₂ (0-0)S(2)	12.28	4	1682	2.76x10 ⁻⁹	9
H ₂ (0-0)S(3)	9.66	5	2504	9.84x10 ⁻⁹	33
H ₂ (0-0)S(4)	8.03	6	3474	2.64x10 ⁻⁸	13
H ₂ (0-0)S(5)	6.91	7	4586	5.88x10 ⁻⁸	45
H ₂ (0-0)S(6)	6.11	8	5829	1.14x10 ⁻⁷	17
H ₂ (0-0)S(7)	5.51	9	7197	2.00x10 ⁻⁷	57

Note. — The statistical weight (g) is $(2J+1)(2I+1)$ where I equals 1 for odd J transitions (ortho transitions) and I equals 0 for even J transitions (para transitions).